Study on the deformation theory of a parabolic part based on solid granules medium forming

Xiang-dong JIA, Chang-cai ZHAO[†‡], Jian-chao LI, Liu-yang HE

(*MOE Key Laboratory of Advanced Forging & Stamping Technology and Science, Yanshan University, Qinhuangdao 066004, China*)

[†]E-mail: zhao1964@ysu.edu.cn

Abstract: Solid granules medium forming (SGMF), a new flexible die forming technology, uses solid granules instead of a rigid male or female die (or elastomer, liquid) for sheet metal drawing. The good fluidity and compressive capacity of a solid granules medium can improve the forming limit of complex shell parts. The sheet metal drawing process of SGMF is a compound process of drawing and bulging, which is very different from the conventional drawing process. A parabolic part is used as the research object for a study of the forming process. Two concepts, drawing weight and bulging weight, are originally proposed in the sheet metal drawing of SGMF (replacing the rigid male die), and the corresponding expressions are obtained. The computational formulas of geometrical conditions and strain in the sheet metal drawing of SGMF are established, and the radius of the strain dividing circle is obtained by calculation. The established theoretical model is applied to the research object, an aircraft part, to analyze the forming process. The results show that the proposed theory can be applied to analyze the strain in different deformation regions of SGMF. This original theory provides a new theoretical analysis for studying the sheet metal drawing of SGMF.

Key words: Solid granules medium; Flexible die forming; Drawing; Drawing weight; Bulging weight; Strain
http://dx.doi.org/10.1631/jzus.A1600408   **CLC number:** TG386

1 Introduction

As industrial technology progresses along with awareness of environmental issues, thin shell parts have become the most commonly selected light-weight structure form, especially the thin shell curved parts, which are widely used in the aerospace and automobile industries.

There are a lot of studies on forming technology for thin shell parts. Dhaiban *et al*. (2014) introduced a new technique for deep drawing of elliptic cups without a blank holder through a conical die. The geometrical parameters of the conical die and punch geometry were studied by numerical simulations and experiments. An elliptic cup with a limit drawing ratio (LDR) of 2.28 had been successfully obtained by applying the proposed technique in an experimental set-up. Tari *et al*. (2013) investigated relevant parameters and the fracture mechanism in a non-isothermal forming process of AZ31B-O magnesium alloy. Gavas and Izciler (2006) presented an innovative blank holder concept. The blank holder was designed as a rigid flat steel plate, on which a tightly wrapped spiral spring is mounted to reduce the friction surface between the blank and the blank holder. As a result, a square cup with a uniform thickness distribution has been obtained. Li *et al*. (2010) pointed out that the shear fracture in advanced high strength steels with reduced ductility could not be predicted by using the concept of forming limit curve. The modified Mohr-Coulomb fracture criterion was recently shown to be applicable to problems involving ductile fracture of materials and sheets.

‡ Corresponding author

 ORCID: Xiang-dong JIA, http://orcid.org/0000-0001-8207-7404;
Chang-cai ZHAO, http://orcid.org/0000-0001-7400-7203

Although much progress has been achieved in conventional drawing, the complexity of shell parts limits, to some extent, the application of conventional technology. The flexible die forming technology has become the main forming method for complex shell parts, taking advantage of its extensive application range and good forming quality.

Hydroforming technology employs hydraulic pressure in sheet metal forming. It has been rapidly developed in the manufacturing of thin shell parts (Lücke *et al.*, 2001). Thiruvarudchelvan and Tan (2006) noted that hydraulic pressure can increase the capability of the basic deep drawing process. Different hydraulic pressures can induce different deep drawing methods. Halkaci *et al.* (2014) successfully enhanced the LDR of AA5754-O from 2.65 to 2.787 by setting up draw beads in the flange. Furthermore, by employing the analysis of variance, it was shown that adding shallow draw beads to the blank holder was the most effective way of using the hydraulic deep drawing process. Labergere and Gelin (2012) used a semi-analytical approach to solve a simplified version of the Navier-Stokes equation. Equations were developed, to calculate the pressure of the fluid film and the leakage volume of the fluid between the sheet and the die in the case of hydromechanical deep drawing. Results showed that it is of great importance to take fluid-structure interactions into account so as to be able to directly evaluate the pressure distribution on the sheet beneath the blank holder. Liu *et al.* (2012) illustrated that the hydraulic pressure is normal to the sheet metal surface in hydroforming, and therefore the normal force equilibrium equation was derived due to the existence of thickness oriented stress. Zhang *et al.* (2015) pointed out that due to the normal stress in the thickness direction caused by the double-sided pressure, the material thickness decreased while the plastic strain and the effective stress increased in the forming region. Thus, a thick shell element can reflect the influence of normal stress in the finite element analysis (FEA) of double-sided hydroforming. Although hydroforming meets the requirements of thin shell parts forming to some degree, there are still some weaknesses. As technology develops, higher standards for the forming of thin shell parts are required.

Viscous medium forming technology has proved to be advantageous in hydroforming, and the tech-nology can also improve the sealing performance of the pressure transfer medium. Shulkin *et al.* (2000) designed a flexible blank holder as part of an experimental viscous pressure forming set-up. This demonstrated that spatial blank holder force control using a viscous medium was instrumental in influencing the material flow in critical forming areas and improving formability of sheet metal parts. Gutscher *et al.* (2004) discovered the interrelationship of the geometric and material parameters under biaxial deformation conditions by employing the finite element method (FEM) simulations and experiments. They also provided the method for determining the flow stress in a biaxial stretching state, in which the internal pressure was employed by the viscous medium in sheet metal forming. Ahmetoglu *et al.* (2004) described the application of viscous pressure forming to the forming of a non-symmetric part from steel, aluminum, and a nickel alloy. They also used FEM simulations and blank holder force control to optimize the process conditions, which can precisely estimate metal flow and distribution thickness. Wang *et al.* (2010) investigated the failure mode of bulge specimens of AA3003 aluminum alloy at various temperatures in a non-isothermal viscous pressure bulging process, using the coupled thermo-mechanical FEM combined with a ductile fracture criterion. It turned out that there are various types of failure modes under different initial temperatures for the viscous medium. Although the viscous medium lowers the demand for sealing during the forming process, its application is still under restrictions like high inner pressure and high temperature.

To overcome the shortcomings of the existing flexible die forming technology, Zhao (2005) first proposed solid granules medium forming (SGMF), which is used for sheet metal drawing using solid granule microspheres instead of a rigid male or female die (or elastomer, liquid). SGMF offers some advantages since the solid granules medium has good fluidity, compressive capacity, and high temperature resistance. It is also sealing-free and recyclable.

Zhao *et al.* (2006) experimentally studied the pressure-transfer performance of the solid granules medium. Results showed that pressure distribution of the solid granules medium along the height direction was uneven. Later experiments on flexible die forming with the method on sheet metal showed that

it was particularly suitable for forming curved surfaces (Zhao *et al.*, 2009). Cao *et al.* (2012) investigated a non-isothermal drawing technology on magnesium alloy sheet based on SGMF. The optimum conditions of AZ31B magnesium alloy forming process were obtained through numerical simulations and experiments. To reduce the risk of fluid medium leakage under high temperature, Grüner and Merklein (2010) trial-manufactured a cup-shaped part using ceramic beads as the pressure-transfer medium and measured pressure-transfer performance of the beads. Dong *et al.* (2015) established the constitutive equation and theoretical forming limit diagram of AA7075 sheet at high temperatures. The sheet forming performance was again analyzed by numerical simulations and experiments. Although much progress with SGMF has been achieved, the deformation mechanism needs further in-depth study to extend its application.

In this study, a parabolic part is chosen as the research object. The geometrical boundary condition and the deformation geometry equations of SGMF are established by analyzing the forming process. The concepts of drawing weight and bulging weight are proposed for the sheet metal drawing of SGMF, and the corresponding expressions are obtained. On this basis, both computational formulas of the geometrical conditions and strain are established. The deformation process of an aerospace part is analyzed both theoretically and experimentally.

2 Parabolic parts forming process based on sheet metal drawing of SGMF

As we have mentioned, SGMF uses solid granules instead of the conventional rigid male die as the new forming medium. The schematic diagram is shown in Fig. 1. The sheet metal is gradually deformed under both axial and radial pressures of solid granules medium, which are caused by a punch.

In the forming process, the deformation regions of the sheet metal can be divided into three regions, i.e., the flange, fillet, and female die regions (Fig. 2). The female die region can be further divided into a part wall region and a free deformation region.

The deformation paths and modes of the whole female die deformation region are shown in Fig. 3.
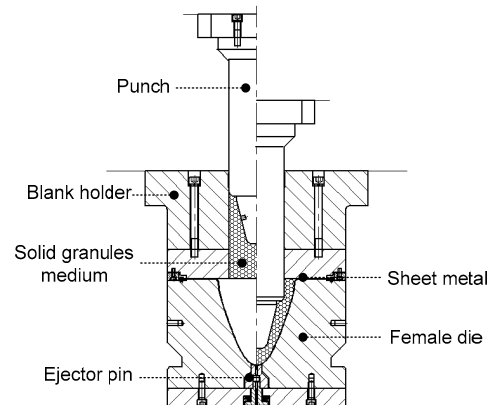

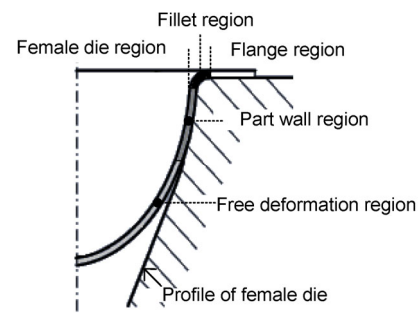**Fig. 1 Schematic diagram of sheet metal drawing based on SGMF**

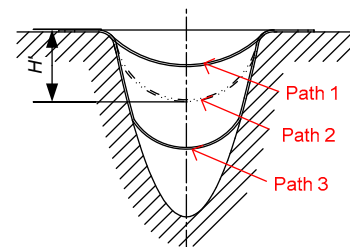**Fig. 2 Deformation regions of the sheet metal**

Fig. 3   Different deformation stages of sheet metal in female die region

1. As shown in Fig. 3, stage 1 is labeled as path 1. When the forming height H is small ($H<H'$), the sheet metal is in contact only with part of the fillet of the female die, and is under free deformation.

2. As shown in Fig. 3, stage 2 is labeled as path 3 and the threshold condition is labeled as path 2. When the forming height H is larger than the forming threshold height H', the sheet metal starts to have contact with the lateral wall of the female die. The deformed sheet metal can be divided into two parts, part wall region and free deformation region. As the

height grows, the free deformation region becomes smaller.

3 Establishment of theoretical model

The deformation process and forming mechanism in the flange region are identical with those during conventional drawing. However, the forming mechanism of the female die region is different, and is formed under the compound action of conventional drawing and bulging.

At a random forming height H, the deformation of any point in the female die region is composed of conventional drawing deformation and bulging deformation. Theoretically, the thickness of sheet metal in the female die region almost keeps invariant during drawing. During the bulging process, the deformation is caused by only thickness reduction of sheet metal and the material in the flange will not flow into the female die. Thus, these are the assumptions we make in this study.

To represent the proportions of drawing deformation and bulging deformation in the whole forming process, the concepts of drawing weight and bulging weight are proposed.

In the flexible drawing technology, drawing weight, α, is defined as the proportion of the deformation caused by drawing to the whole deformation in the female die region. Bulging weight, β, is defined as the proportion of the deformation caused by bulging to the whole deformation in the female die region.

During the forming process of parabolic parts, sheet metal drawing is first generated. In this stage, the flange radius decreases. After the drawing, the flange is unchanged, and the sheet metal in the female die region bulges due to the inner pressure of the solid granules medium. Then the forming height continually increases but the thickness decreases. As a result, in the whole deformation process, the drawing weight (α) and bulging weight (β) can be expressed as functions of the workpiece surface area variation before and after deformation:

$$\alpha = f_1(\Delta S) = \frac{\Delta S_d}{\Delta S_a} = \frac{\Delta S_f}{\Delta S_a}, \tag{1}$$

$$\beta = f_2(\Delta S) = \frac{\Delta S_b}{\Delta S_a}, \tag{2}$$

where ΔS_f is equivalent to the decrement of the flange surface area (i.e., the ratio of decrement of the flange volume to the initial thickness), ΔS_d the surface area increment of the workpiece in the female die region under drawing, ΔS_b the surface area increment of the workpiece in the female die region under bulging, and ΔS_a the surface area increment of the workpiece in the female die region. $\Delta S_a = S_a - \pi R_d^2 = \Delta S_d + \Delta S_b$, where S_a is the surface area of the workpiece in the female die region.

When the deformation is formed only by drawing, $\Delta S_b = 0$, $\Delta S_f = \Delta S_a$, namely, $\alpha = 1$.

When the deformation is formed only by bulging, $\Delta S_f = 0$, $\Delta S_b = \Delta S_a$, namely, $\beta = 1$.

When the deformation is formed by both drawing and bulging in one forming process, the relationship of drawing weight (α) and bulging weight (β) conforms to the condition shown below:

$$\alpha + \beta = 1. \tag{3}$$

3.1 Basic assumptions and geometrical conditions

An arbitrary parabolic shaped shell part is chosen as the research object, with height b and opening radius R_d. The cylinder coordinate system is set to analyze the part. As shown in Fig. 4, the center of the workpiece opening plane is set as the origin of the coordinates, the axis of symmetry is set as h-axis, and the line perpendicular to the axis of symmetry in the opening plane is set as the r-axis. The generatrix equation of the parabolic part can be obtained as

$$h = ar^2 - b, \tag{4}$$

where r is the radius of a random point in generatrix of the parabolic part, b the height of the parabolic part, and $a = b/R_d^2$.

To simplify the calculation and application of the theoretical model, the following assumptions are made:

1. The thickness of the flange remains constant during deformation. The deformation of the female die region is a compound of conventional drawing and bulging, which work separately. First, sheet metal is deformed by drawing, and the outer radius of the flange decreases from R_0 to R_w. The thickness of the sheet metal in the flange region and female die region

remains constant. Then sheet metal in the female die region is deformed by bulging alone, with the radius and thickness of the flange remaining constant.
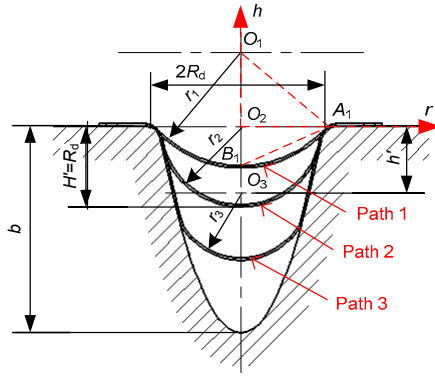

Fig. 4 Deformation stages of parabolic shaped shell part

2. The shape of the free deformation region is assumed here as a spherical cap. Large numbers of forming experiments conducted by our research team showed that the generatrix shape of the formed workpiece by SGMF in the free deformation region can be fitted by a circular function.

3. When the forming height is not larger than the opening radius of the female die (R_d), the sheet metal is assumed in contact only with the fillet of the female die and produces free forming only, which is labeled as path 1 in Fig. 4. Until the whole hemisphere is formed, the radius of the hemisphere equals the forming height and it also equals the opening radius of the female die (R_d). The situation is labeled as path 2 in Fig. 4.

4. When the forming height is larger than the opening radius of the female die (R_d), the deformation of the female die region is assumed to consist of 1/2 spherical shell and part wall revolving shell, which is labeled as path 3 in Fig. 4.

Some geometrical relationships based on the fundamental assumptions can be obtained as follows.

When the forming height satisfies $H \leq R_d$, and within $\triangle O_1 A_1 B_1$ and $\triangle O_1 O_2 A_1$, $r_1^2 = R_d^2 + (r_1 - H)^2$, the radius of the spherical cap (r_1) can be derived as

$$r_1 = \frac{R_d^2 + H^2}{2H}. \tag{5}$$

When the forming height satisfies $H > R_d$, the height of the spherical shell center is assumed as h',

and then $h' + r_3 = |ar_3^2 - b| + r_3 = H$. The radius of spherical cap (r_3) can be derived as

$$r_3 = \frac{1 + \sqrt{1 + 4a(b - H)}}{2a}. \tag{6}$$

3.2 Deformation analysis of flange region

The initial outer radius of the sheet metal is R_0, and it decreases to R_w when the sheet metal, under the pressure of solid granules medium and with an initial thickness t_0, is processed to the forming height H. A point on the circle with radius R_1 of the initial sheet metal will move to the circle with radius R on the flange of the workpiece (Fig. 5).
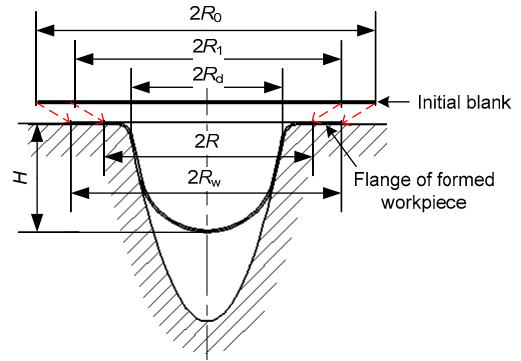

Fig. 5 Deformation of flange during deep drawing

According to the constant volume condition, the equation can be obtained as

$$\pi(R_0^2 - R_1^2) \cdot t_0 = \pi(R_w^2 - R^2) \cdot t_0. \tag{7}$$

From Eq. (7), we have

$$R_1 = \sqrt{R_0^2 - R_w^2 + R^2}. \tag{8}$$

According to the definition of the strain, the tangential strain in any radius (R) of the formed workpiece flange can be expressed as

$$\varepsilon_\theta = \ln \frac{2\pi R}{2\pi R_1} = \ln \frac{R}{\sqrt{R_0^2 - R_w^2 + R^2}}. \tag{9}$$

The thickness of the flange is assumed to be constant during deformation. According to the

constant volume condition, the radial strain of the points on the circle, with radius R, of the flange region can be obtained as

$$\varepsilon_r = -\varepsilon_\theta = -\ln \frac{R}{\sqrt{R_0^2 - R_w^2 + R^2}}. \tag{10}$$

3.3 Deformation analysis of female die region

The forming mechanism of parabolic parts based on SGMF is different from that of conventional drawing. The deformation of sheet metal in the female die region is the result of both conventional drawing and bulging, and it cannot be directly analyzed by existing theories. To make theoretical analysis of the whole deformation process, a single deformation analysis method is adopted; namely, the single drawing is defined as the sheet metal deformed only by the action of conventional drawing, and the single bulging is defined as the sheet metal deformed only by the action of conventional bulging. The deformation analysis can be respectively analyzed under single drawing and single bulging conditions. Also, the actual deformation can be calculated with the drawing weight and bulging weight.

3.3.1 Deformation analysis with forming height $H \leq R_d$

The sheet metal in the female die region produces free deformation only when the forming height is $H \leq R_d$. It is assumed that point O in the formed workpiece is moved from the initial position point O' in the initial sheet metal under the compound action of drawing and bulging (Fig. 6).

3.3.1.1 Drawing weight and bulging weight

Based on the fundamental assumptions, when the outer radius of the flange decreases from R_0 to R_w, the surface area decrement of the flange can be calculated as

$$\Delta S_f = \pi \left(R_0^2 - R_w^2 \right). \tag{11}$$

The surface area variation of the female die region is

$$\Delta S_a = \pi \left(2r_1 H - R_d^2 \right) = \pi H^2, \tag{12}$$

where r_1 is derived from Eq. (5).

Substituting Eqs. (11) and (12) into Eqs. (1) and (3), the drawing weight and bulging weight can be obtained as follows:

$$\alpha = \frac{\Delta S_f}{\Delta S_a} = \frac{R_0^2 - R_w^2}{H^2}, \tag{13}$$

$$\beta = 1 - \frac{\Delta S_f}{\Delta S_a} = 1 - \frac{R_0^2 - R_w^2}{H^2}. \tag{14}$$

3.3.1.2 Analysis of single drawing deformation

Under the action of single drawing, the sheet metal is deformed to the shape with the forming height H in Fig. 6. The corresponding formed point of the initial point O'_1 in the sheet metal is point O in the spherical cap of the formed workpiece (Fig. 7).
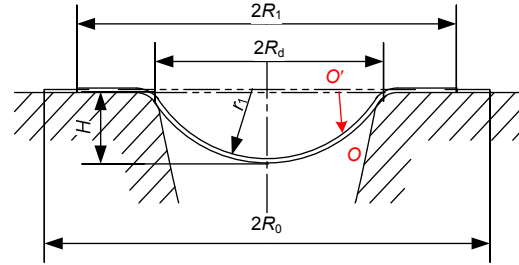

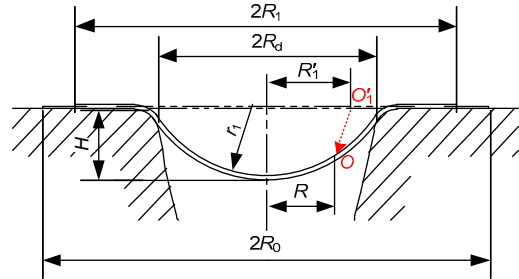**Fig. 6 Deformation of sheet metal with forming height $H \leq R_d$**

Fig. 7 Single drawing deformation ($H \leq R_d$)

Based on the fundamental assumptions, the thickness variation of sheet metal is ignored. With respect to the constant volume condition, we have

$$\pi \left(R'_1 \right)^2 \cdot t_0 = 2\pi r_1 \cdot \left(r_1 - \sqrt{r_1^2 - R^2} \right) \cdot t_0. \tag{15}$$

Then

$$R'_1 = \sqrt{2r_1 \cdot \left(r_1 - \sqrt{r_1^2 - R^2} \right)}. \tag{16}$$

The tangential strain of point O can be obtained as

$$\varepsilon_\theta^d = \ln \frac{2\pi R}{2\pi R'_1} = \ln \frac{R}{\sqrt{2r_1 \cdot \left(r_1 - \sqrt{r_1^2 - R^2} \right)}}. \tag{17}$$

Substituting Eq. (5) into Eq. (17),

$$\varepsilon_\theta^d = \ln \frac{2HR}{\sqrt{2\left(R_d^2 + H^2\right)^2 - \left(R_d^2 + H^2\right)\sqrt{\left(R_d^2 + H^2\right)^2 - 4H^2R^2}}}. \tag{18}$$

According to the constant volume condition, the radial strain of point O along the generatrix can be derived as

$$\varepsilon_r^d = -\varepsilon_\theta^d. \tag{19}$$

3.3.1.3 Analysis of single bulging deformation

Assume that a sheet metal, with an initial radius R_0, is formed to the shape of a parabolic part with the forming height H by the action of bulging and no fracture occurring. Point O_2', in radius R_2', of the initial sheet metal moves to point O in the spherical cap of the formed workpiece after the action of single bulging (Fig. 8).
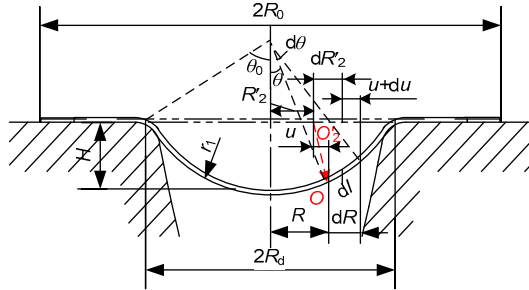

Fig. 8 Single bulging deformation ($H \le R_d$)

Based on the fundamental assumptions, the shape of the free deformation region (Fig. 8) is a spherical cap. According to the geometric equation of axisymmetrical deformation, the tangential strain ε_θ^b and radial strain ε_r^b of point O can be expressed as

$$\varepsilon_\theta^b = \varepsilon_r^b = \ln \frac{R}{R-u} = \ln \frac{dR}{(dR - du)\sin\theta}. \tag{20}$$

Thus, the following equation can be obtained:

$$\frac{R}{R-u} = \frac{dR}{(dR - du)\sin\theta}. \tag{21}$$

According to the geometric condition, $R = r_1\sin\theta$, and $dR = r_1\cos\theta d\theta$. Substituting them into Eq. (21), we have

$$\frac{du}{d\theta} - \frac{u}{\sin\theta} = r_1(\cos\theta - 1). \tag{22}$$

Then, u can be obtained by solving Eq. (22):

$$u = \frac{\sin\theta}{\cos\theta + 1}(r_1\cos\theta + C), \tag{23}$$

where C is a constant of integration.

At the fillet of the female die, where $R = R_d$, $\sin\theta_0 = R_d/r_1$, and $u = 0$, substitute them into Eq. (23). Then $C = -r_1\cos\theta_0$ and Eq. (23) becomes

$$u = \frac{R}{\cos\theta + 1}(\cos\theta - \cos\theta_0). \tag{24}$$

According to the geometric condition, Eq. (24) can be expressed as

$$u = \frac{R}{\sqrt{r_1^2 - R^2} + r_1}\left(\sqrt{r_1^2 - R^2} - \sqrt{r_1^2 - R_d^2}\right). \tag{25}$$

Substituting Eq. (25) into Eq. (20), the tangential strain ε_θ^b and radial strain ε_r^b of point O can be obtained as

$$\varepsilon_r^b = \varepsilon_\theta^b = \ln \frac{\sqrt{r_1^2 - R^2} + r_1}{r_1 + \sqrt{r_1^2 - R_d^2}}. \tag{26}$$

The normal strain in the thickness direction of point O can be obtained based on the constant volume condition:

$$\varepsilon_t^b = -2\ln \frac{\sqrt{r_1^2 - R^2} + r_1}{r_1 + \sqrt{r_1^2 - R_d^2}}. \tag{27}$$

3.3.1.4 Deformation analysis of sheet metal based on SGMF

With the solid granules medium, sheet metal is deformed to the shape with the forming height H in Fig. 6 by the compound action of conventional drawing and bulging. Consequently, the strain of point O of the free deformation region in radius R can be obtained as follows:

$$\varepsilon_\theta = \alpha\varepsilon_\theta^d + \beta\varepsilon_\theta^b \quad (H \le R_d), \tag{28}$$

$$\varepsilon_r = \alpha\varepsilon_r^d + \beta\varepsilon_r^b \quad (H \le R_d), \tag{29}$$

$$\varepsilon_t = \beta \varepsilon_\theta^b \quad (H \leq R_d). \tag{30}$$

Therefore, the thickness t of any point on the formed workpiece can be expressed as

$$t = \exp(\varepsilon_t) t_0 \quad (H \leq R_d). \tag{31}$$

3.3.2 Deformation analysis with forming height $H > R_d$

When the forming height satisfies $H > R_d$, the sheet metal gradually comes into contact with the die under internal pressure of the solid granules medium. The deformation region of the female die consists of a part wall region and a free deformation region. Point A is assumed as a random point in the free deformation region and it moves from point A' in the initial sheet metal under the compound action of drawing and bulging. Point B is assumed as a random point in the part wall region and it moves from point B' in the initial sheet metal under the compound action of drawing and bulging (Fig. 9).

3.3.2.1 Drawing weight and bulging weight

According to the fundamental assumptions, when the outer radius of the flange decreases from R_0 to R_w, the surface area decrement of the flange, ΔS_f, can be obtained from Eq. (11) under the condition shown in Fig. 9. The surface area of the female die region can be calculated as

$$S_a = \frac{\pi}{6a^2}\left[\sqrt{\left(4a^2 R_d^2 + 1\right)^3} - \sqrt{\left(4a^2 r_3^2 + 1\right)^3}\right] + 2\pi r_3^2, \tag{32}$$

where r_3 can be obtained from Eq. (6). According to Eq. (32), the surface area variation of the female die region can be obtained as

$$\Delta S_a = S_a - \pi R_d^2$$
$$= \frac{\pi}{6a^2}\left[\sqrt{\left(4a^2 R_d^2 + 1\right)^3} - \sqrt{\left(4a^2 r_3^2 + 1\right)^3}\right] + \pi\left(2r_3^2 - R_d^2\right). \tag{33}$$

Consequently, the drawing weight and bulging weight under the condition of Fig. 9 can be calculated:

$$\alpha = \frac{\Delta S_f}{\Delta S_a} = \frac{\pi\left(R_0^2 - R_w^2\right)}{S_a - \pi R_d^2}, \tag{34}$$

$$\beta = 1 - \frac{\Delta S_f}{\Delta S_a} = 1 - \frac{\pi\left(R_0^2 - R_w^2\right)}{S_a - \pi R_d^2}. \tag{35}$$

3.3.2.2 Deformation analysis of single drawing

Assume that the sheet metal is deformed to the workpiece shape with a forming height H (Fig. 10), by single drawing. Assume no thickness variation occurred in the part wall or free deformation region.
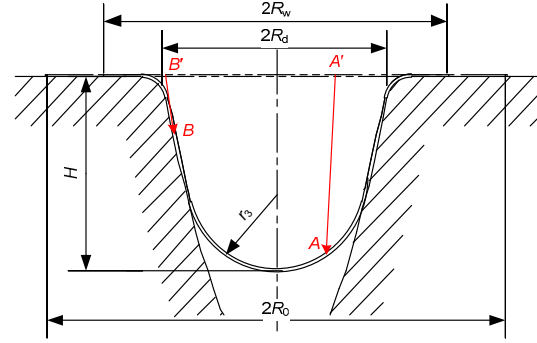

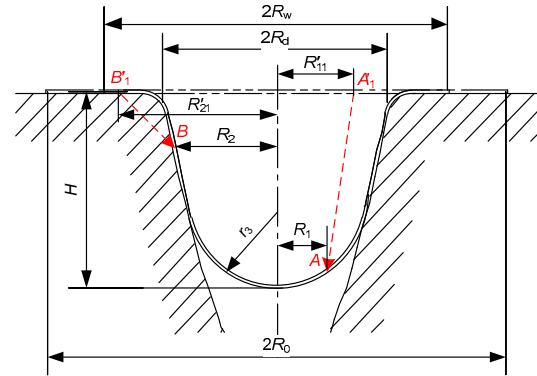**Fig. 9 Deformation of sheet metal with forming height $H > R_d$**

Fig. 10 Single drawing deformation ($H > R_d$)

Point A on the circle with radius R_1 ($0 < R_1 \leq r_3$) of the free deformation region moves from point A'_1 of the initial sheet metal. From Eqs. (18) and (19), and with respect to the constant volume condition, the tangential and radial strain of point A can be obtained:

$$\varepsilon_\theta^d = \ln \frac{2\pi R_1}{2\pi R'_{11}} = \ln \frac{R_1}{\sqrt{2r_3 \cdot \left(r_3 - \sqrt{r_3^2 - R_1^2}\right)}}, \tag{36}$$

$$\varepsilon_r^d = -\varepsilon_\theta^d, \tag{37}$$

where R'_{11} is the radius of point A'_1 and r_3 is the radius of the spherical cap of the free deformation region with forming height $H > R_d$, satisfying Eq. (6).

Point B on the circle with radius R_2 ($r_3 < R_2 < R_d$) of the part wall region moves from point B'_1 of the initial

sheet metal. According to the constant volume condition, we have

$$\pi (R'_{21})^2 t_0 = 2\pi r_3^2 t_0$$
$$+ \left[\frac{\pi}{6a^2} \sqrt{\left(4a^2 R_2^2 +1\right)^3} - \frac{\pi}{6a^2} \sqrt{\left(4a^2 r_3^2 +1\right)^3} \right] t_0, \quad (38)$$

where R'_{21} is the radius of point B'_1. Then

$$R'_{21} = \frac{1}{\sqrt{6}a} \sqrt{12a^2 r_3^2 + \sqrt{\left(4a^2 R_2^2 +1\right)^3} - \sqrt{\left(4a^2 r_3^2 +1\right)^3}}.$$
$$(39)$$

According to Eq. (39), the tangential strain of point B can be calculated as

$$\varepsilon_\theta^d = \ln \frac{2\pi R_2}{2\pi R'_{21}} = \ln \frac{\sqrt{6}a R_2}{\sqrt{12a^2 r_3^2 + \sqrt{\left(4a^2 R_2^2 +1\right)^3} - \sqrt{\left(4a^2 r_3^2 +1\right)^3}}}.$$
$$(40)$$

Then the radial strain along the generatrix of point B can be obtained:

$$\varepsilon_r^d = -\varepsilon_\theta^d. \quad (41)$$

3.3.2.3 Deformation analysis of single bulging

Assume that the sheet metal can be formed into any forming height without fracture. The shape shown in Fig. 11 is formed by single bulging deformation.
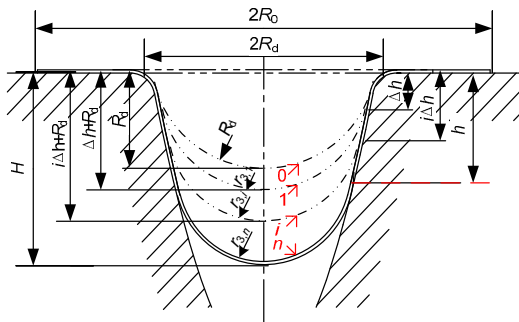

Fig. 11 Single bulging deformation ($H>R_d$)

According to the geometric condition, the height of part wall region h can be calculated as

$$h=H-R_d. \quad (42)$$

In the single bulging process, the sheet metal in the part wall region is tightly attached to the female die because of the pressure from the granules medium, and, for the most part, remains consistent in the following forming. However, the thickness of the bottom free deformation region continues to decrease and generates a new part wall region and free deformation region in the forming process that follows.

The whole attaching-die process can be divided into n steps (Fig. 11). The height of the newly generated part wall region in each step Δh is

$$\Delta h=H-R_d/n. \quad (43)$$

Half of the spherical shell is first generated before the sheet metal attaches to the female die, as position 0 in Fig. 11. In this status, according to Eqs. (26) and (27), the radial strain $\varepsilon_{r,0}^b$, tangential strain $\varepsilon_{\theta,0}^b$, and normal strain $\varepsilon_{t,0}^b$ of any point in position 0 can be obtained:

$$\varepsilon_{r,0}^b = \varepsilon_{\theta,0}^b = \ln \frac{\sqrt{R_d^2 - R^2} + R_d}{R_d} \quad (0<R \le R_d), \quad (44)$$

$$\varepsilon_{t,0}^b = 2\ln \frac{R_d}{\sqrt{R_d^2 - R^2} + R_d} \quad (0<R \le R_d). \quad (45)$$

When the forming height increases from R_d to $R_d+\Delta h$, the newly generated height of the part wall region is Δh, as shown at position 1 in Fig. 11. Assume that the thickness of free deformation region decreases uniformly while the sheet metal bulges from position 0 to position 1; i.e., the increment of normal strain at any point is equal. According to the constant volume condition, the increment of normal strain in the thickness direction $\Delta \varepsilon_{m,1}^b$ from position 0 to position 1 can be obtained:

$$\Delta \varepsilon_{m,1}^b = \ln \Delta t_{m,1} = \ln \frac{S_0^f}{S_1}, \quad (46)$$

where S_0^f is the surface area of the workpiece in the free deformation region at position 0, and S_1 is the surface area of the workpiece in the female die region at position 1. According to the geometric condition, we have

$$S_0^f = 2\pi R_d^2, \quad (47a)$$

$$S_1 = 2\pi R_d^2 + \frac{\pi}{6a^2} \sqrt{\left(4a^2 R_d^2 +1\right)^3} - \frac{\pi}{6a^2} \sqrt{\left(4a^2 r_{3,1}^2 +1\right)^3}.$$
$$(47b)$$

From Eq. (6), $r_{3,1}$ can be calculated as

$$r_{3,1} = \frac{1 + \sqrt{1 + 4a(b - R_d - \Delta h)}}{2a}. \qquad (48)$$

According to Eqs. (45) and (46), for any point at position 1 in the free deformation region with radius R, the normal strain in the thickness direction $\varepsilon^{bf}_{t,1}$ can be obtained:

$$\varepsilon^{bf}_{t,1} = \varepsilon^{b}_{t,0} + \Delta\varepsilon^{b}_{m,1} \quad (0 < R \le r_{3,1}). \qquad (49)$$

In the single bulging process, the tangential strain and radial strain satisfy $\varepsilon_\theta = \varepsilon_r$. According to the constant volume condition and Eq. (49), the tangential strain $\varepsilon^{bf}_{\theta,1}$ and radial strain $\varepsilon^{bf}_{r,1}$ of any point at position 1 in free deformation region can be calculated as

$$\varepsilon^{bf}_{r,1} = \varepsilon^{bf}_{\theta,1} = -\frac{1}{2}\left(\varepsilon^{b}_{t,0} + \Delta\varepsilon^{b}_{m,1}\right) \quad (0 < R \le r_{3,1}). \qquad (50)$$

Since the newly generated height of the part wall region Δh is quite small, assume that the strains of any point within the range of Δh are equal, with values being equal to the ones of the point on the circle with radius $r_{3,1}$ in the free deformation region. According to Eqs. (49) and (50), the strains within the range of Δh in this newly generated part wall region can be obtained:

$$\varepsilon^{bt}_{t,1} = \varepsilon^{bf}_{t,1}\Big|_{R=r_{3,1}}, \qquad (51)$$

$$\varepsilon^{bt}_{r,1} = \varepsilon^{bt}_{\theta,1} = -\frac{1}{2}\varepsilon^{bt}_{t,1}. \qquad (52)$$

Similarly, the newly generated part wall region and free deformation region in position i are bulged from the free deformation region in position $i-1$. In this process, the increment of the normal strain in the thickness direction $\Delta\varepsilon^{b}_{m,i}$ can be calculated:

$$\Delta\varepsilon^{b}_{m,i} = \ln\frac{S^{f}_{i-1}}{S_i}, \qquad (53)$$

where S^{f}_{i-1} is the surface area of the workpiece in the free deformation region at position $i-1$, and S_i is the surface area of the workpiece in the female die region at position i. Thus, we have

$$S^{f}_{i-1} = 2\pi r^2_{i-1}, \qquad (54a)$$

$$S_i = 2\pi r^2_{3,i} + \frac{p}{6a^2}\sqrt{\left(4a^2 r^2_{3,i-1} + 1\right)^3} - \frac{\pi}{6a^2}\sqrt{\left(4a^2 r^2_{3,i} + 1\right)^3}. \qquad (54b)$$

From Eq. (6), we have

$$r_{3,i} = \frac{1 + \sqrt{1 + 4a(b - R_d - i\Delta h)}}{2a} \quad (0 < i \le n). \qquad (55)$$

The normal strain in the thickness direction $\varepsilon^{bf}_{t,i}$ can be obtained:

$$\varepsilon^{bf}_{t,i} = \varepsilon^{bf}_{t,i-1} + \Delta\varepsilon^{b}_{m,i} = \varepsilon^{b}_{t,0} + \Delta\varepsilon^{b}_{m,1} + \cdots + \Delta\varepsilon^{b}_{m,i} \quad (0 < R \le r_{3,i}). \qquad (56)$$

Given that the tangential strain and radial strain satisfy the relation in the single bulging process, we have

$$\varepsilon^{bf}_{r,i} = \varepsilon^{bf}_{\theta,i} = -\frac{1}{2}\left(\varepsilon^{b}_{t,0} + \Delta\varepsilon^{b}_{m,1} + \cdots + \Delta\varepsilon^{b}_{m,i}\right) \quad (0 < R \le r_{3,i}). \qquad (57)$$

Thus, the strains (the normal strain in the thickness direction $\varepsilon^{bt}_{t,i}$, tangent strain $\varepsilon^{bt}_{\theta,i}$, and radial strain $\varepsilon^{bt}_{r,i}$) of the newly generated part wall region can be calculated:

$$\varepsilon^{bt}_{t,i} = \varepsilon^{bf}_{t,i}\Big|_{R=r_{3,i}}, \qquad (58)$$

$$\varepsilon^{bt}_{r,i} = \varepsilon^{bt}_{\theta,i} = -\frac{1}{2}\varepsilon^{bt}_{t,i}. \qquad (59)$$

According to Eqs. (56) and (57), when the forming height reaches H, the bulging strains in the free deformation region can be obtained:

$$\varepsilon^{bf}_{t,n} = \varepsilon^{b}_{t,0} + \Delta\varepsilon^{b}_{m,1} + \cdots + \Delta\varepsilon^{b}_{m,i} + \cdots + \Delta\varepsilon^{b}_{m,n} \quad (0 < R \le r_{3,n}), \qquad (60)$$

$$\varepsilon^{bf}_{r,n} = \varepsilon^{bf}_{\theta,n} = -\frac{1}{2}\left(\varepsilon^{b}_{t,0} + \Delta\varepsilon^{b}_{m,1} + \cdots + \Delta\varepsilon^{b}_{m,i} + \cdots + \Delta\varepsilon^{b}_{m,n}\right) \quad (0 < R \le r_{3,n}). \qquad (61)$$

The strains of any point in the part wall region can be obtained from Eqs. (58) and (59).

3.3.2.4 Deformation analysis of sheet metal based on SGMF

In the forming process with solid granules medium, any point in the female die region of the workpiece shown in Fig. 9 is the result of the compound action of drawing and bulging. Consequently, when the forming height satisfies $H>R_d$, the tangential strain, the radial strain, and the normal strain in the thickness direction of a random point in the female die region can be obtained:

$$\varepsilon_\theta = \alpha\varepsilon_\theta^d + \beta\varepsilon_\theta^b \quad (H>R_d), \tag{62a}$$

$$\varepsilon_r = \alpha\varepsilon_r^d + \beta\varepsilon_r^b \quad (H>R_d), \tag{62b}$$

$$\varepsilon_t = \beta\varepsilon_\theta^b \quad (H>R_d). \tag{62c}$$

In Eqs. (62a)–(62c), when the radial radius of a random point, R, satisfies $0<R\leq r_3$, the point is in the free deformation region. Its radial strain and tangential strain can be derived from Eqs. (36), (37), (60), and (61). When R satisfies $r_3<R<R_d$, the point is in the part wall region. Its radial strain and tangential strain can be derived from Eqs. (40), (41), (58), and (59).

The thickness t of any point on the formed workpiece can be calculated with Eq. (62c):

$$t=\exp(\varepsilon_t)t_0 \quad (H>R_d). \tag{63}$$

From Eqs. (13), (14), (34), and (35), the drawing weight (α) and bulging weight (β) are functions relating to the radius of the sheet metal (R_0), the outer radius of the flange (R_w), and the forming height (H). At a certain forming height, the smaller the ratio of the outer radius of the formed workpiece flange to the initial outer radius of sheet metal (namely, R_w/R_0) is, the larger the proportion of the drawing weight in the whole deformation is, and the smaller the thickness reduction of sheet metal in the deformation region is. Conversely, the thickness reduction of sheet metal in the deformation region is larger.

When the ratio of the outer radius of the flange of the workpiece to the outer radius of the sheet metal (namely, R_w/R_0) is fixed, the drawing weight decreases with the increment of the forming height. The drawing weight reaches the minimum value when the forming height increases to a critical value. In the critical condition, the whole sheet metal acts only with bulging deformation, and the thickness in the deformation region will reduce gradually, causing easy fracture in the free deforming region.

4 Deformation analysis of the deep drawing process of an aircraft part

As shown in Fig. 12, the aircraft part is a complex thin-walled shell part, whose profile generatrix can be fitted by a parabolic function. In the coordinates shown in Fig. 12, the equation of the parabolic function is expressed as

$$h = 0.0197r^2 - 211. \tag{64}$$

The aircraft part is made from 1Cr18Ni9Ti sheet by cold rolling and its thickness is 1.2 mm. The basic mechanical parameters are shown in Table 1.

4.1 Theoretical analysis

To analyze the deformation process of SGMF shown in Fig. 12 by applying the theoretical model described in Section 2, the outer radius of the flange was measured at different drawing heights. When the measured values were substituted into the
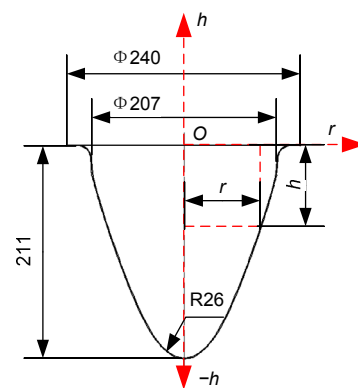

Fig. 12 Target part of the certain aircraft part

Table 1 Mechanical parameters of 1Cr18Ni9Ti

Density, ρ (g/cm³)	Elastic modulus, E (GPa)	Poisson's ratio, μ	Yield strength, σ_s (MPa)	Tensile strength, σ_b (MPa)	Elongation rate, δ(%)
7.85	200	0.28	≥250	≥1000	≥50

corresponding calculation formulas, theoretical results of drawing weight, bulging weight, and strain distribution regularities were obtained. The forming experiments were conducted by the forming equipment and mould (Fig. 13).

Computer programs can be used to analyze the sheet metal drawing process with theoretical formulas. In this study, the theoretical program of the parabolic part was designed with the MATLAB programming language. The program structure diagram is shown in Fig. 14.

Fig. 13 Experimental equipment and mould

4.2 Analysis of deep drawing process

Under the same conditions (R_0=365 mm, t_0= 1.2 mm, and H=80 mm), the drawing process was carried out with three lubrication media (nothing, oil, and water-based graphite). The maximum thickness reduction rate (namely, $\Delta t/t_0$, where Δt is the difference between the minimum thickness and the initial thickness, and t_0 is the initial thickness of sheet metal) of the formed workpiece is obtained (Table 2).

It turned out that the maximum thickness reduction rate with lubrication is smaller than that of no lubrication at the same forming height. However, pressure from the granules medium makes it easier for oil to be squeezed out, especially at the fillet of the female die. Thus, the effect of oil lubrication is greatly reduced. When using water-based graphite lubrication, a layer of graphite thin film will be formed on the surface of the blank, and it is difficult

Table 2　Maximum thickness reduction rate with different lubrication conditions (H=80 mm)

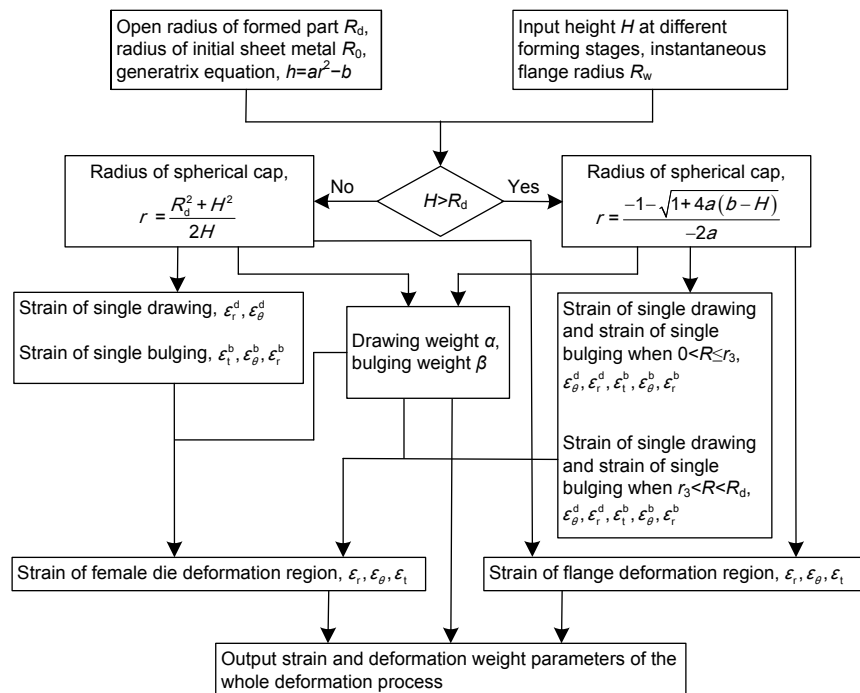| Lubrication condition	Maximum reduction rate (%)
Nothing	31.40
Oil	20.10
Water-based graphite	14.30

Fig. 14 Program structure diagram of theoretical calculation

to squeeze out graphite even under high pressure. So, the friction between the blank and die can be signally reduced. Thus, the water-based graphite is used as the lubrication medium in this study.

The initial diameter of the sheet metal is 365 mm, and it is processed using water-based graphite as the lubricant. The experimental results of instantaneous outer radius R_w of the flange and forming height H at different stages are shown in Table 3.

Table 3 Geometry size of workpiece

Blank holder gap (mm)	Height, H (mm)	Average radius of flange, R_w (mm)
1.0t_0	38.3	181.0
	66.0	178.3
	85.0	176.4
	102.0	Fracture
1.1t_0	38.0	179.0
	70.8	170.5
	105.5	157.0
	138.0	148.5
1.2t_0	38.2	179.8
	67.5	173.5
	99.5	162.7
	138.0	152.0

Substituting the experimental data of Table 3 into the theoretical calculation program, the deformation weight parameters were obtained and are shown in Fig. 15.

With the same forming height, it can be seen from Fig. 15 that the drawing weight in the deformation increases when the blank holder gap (BHG) increases from 1.0t_0 to 1.1t_0. However, the drawing weight in the deformation decreases when the BHG increases from 1.1t_0 to 1.2t_0. At the same BHG, the drawing weight decreases with the increase of the forming height. In the whole forming process, the change of the bulging weight is contrary to the drawing weight.

The following process was carried out: cut the workpiece into two halves along the middle section; next, create coordinates and label measurement points in this cutting plane and mark those point positions through the height gauge and caliper (Fig. 16); then measure the thickness with the measuring equipment of Fig. 17.
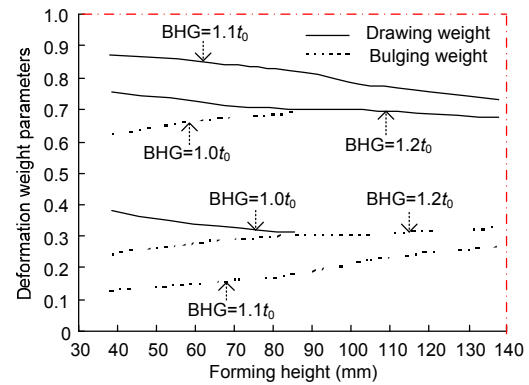

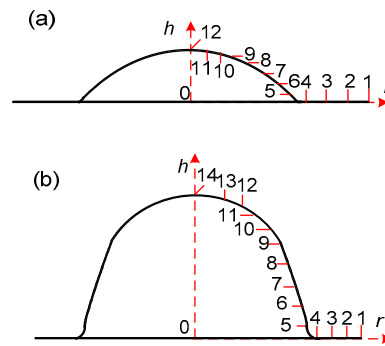**Fig. 15 Curves of deformation weight parameters**

Fig. 16 Positions of measurement points
(a) H=38 mm; (b) H=138 mm

Fig. 17 Thickness measuring equipment

In the measurement process, the thickness of the flange outer edge (point 1 in Fig. 16) is first measured by the vernier caliper and used as the measuring basis of other measurement points. Then the variation value relative to point 1 can be obtained through the dial indicator with the measuring equipment in Fig. 17. Thus, the thickness of the corresponding point can be

obtained by making subtractions of the basis value of point 1 and the measured relative value.

To minimize the measurement error caused by human factors, three measurements were performed for the same workpiece. The measurement results of measurement points are shown in Tables 4 and 5.

Combining the experimental measurement (the average values in Tables 4 and 5) and theoretical calculation, the curves of the maximum thickness reduction rate of the formed workpiece at different forming heights and BHGs are shown in Fig. 18. The thickness distribution curves of workpieces at the same forming height (H=38 mm, H=138 mm) and

different BHGs are shown in Fig. 19. The experimental value is the average of the three measurement results in Tables 4 and 5.

It can be seen from Figs. 18 and 19 that the maximum thickness reduction rate of the formed workpiece increases with the increment of forming height. At the same forming height, the maximum thickness reduction rate in the deformation decreases when BHG increases from $1.0t_0$ to $1.1t_0$. However, when BHG increases from $1.1t_0$ to $1.2t_0$, excessive BHG makes serious wrinkles in the flange and the maximum thickness reduction rate in the deformation increases.

Table 4 Thickness of workpiece for different measurement points (H=38 mm) (unit: mm)

Point	BHG=$1.0t_0$				BHG=$1.1t_0$				BHG=$1.2t_0$			
	No. 1	No. 2	No. 3	Average	No. 1	No. 2	No. 3	Average	No. 1	No. 2	No. 3	Average
1	1.20	1.20	1.21	1.203	1.21	1.21	1.21	1.210	1.21	1.21	1.22	1.213
2	1.20	1.19	1.19	1.193	1.20	1.21	1.21	1.207	1.21	1.20	1.21	1.207
3	1.20	1.19	1.20	1.197	1.20	1.21	1.20	1.203	1.20	1.21	1.20	1.203
4	1.19	1.20	1.19	1.193	1.20	1.20	1.20	1.200	1.20	1.20	1.19	1.197
5	1.18	1.19	1.18	1.183	1.20	1.19	1.20	1.197	1.18	1.17	1.19	1.180
6	1.12	1.11	1.11	1.113	1.18	1.18	1.18	1.180	1.15	1.14	1.15	1.147
7	1.08	1.09	1.09	1.087	1.17	1.17	1.18	1.173	1.13	1.14	1.12	1.130
8	1.05	1.05	1.04	1.047	1.17	1.16	1.17	1.167	1.10	1.09	1.10	1.097
9	1.03	1.04	1.03	1.033	1.17	1.16	1.17	1.167	1.10	1.09	1.09	1.093
10	1.03	1.03	1.02	1.027	1.16	1.15	1.15	1.153	1.09	1.08	1.09	1.087
11	1.02	1.02	1.02	1.020	1.15	1.14	1.14	1.143	1.08	1.08	1.08	1.080
12	1.01	1.02	1.01	1.013	1.14	1.14	1.14	1.140	1.08	1.07	1.08	1.077

BHG: blank holder gap

Table 5 Thickness of workpiece for different measurement points (H=138 mm) (unit: mm)

| Point	BHG=$1.1t_0$				BHG=$1.2t_0$			
	No. 1	No. 2	No. 3	Average	No. 1	No. 2	No. 3	Average
1	1.22	1.22	1.21	1.217	1.22	1.22	1.21	1.217
2	1.22	1.21	1.21	1.213	1.21	1.21	1.22	1.213
3	1.21	1.20	1.20	1.203	1.21	1.20	1.21	1.207
4	1.20	1.20	1.19	1.197	1.20	1.18	1.19	1.190
5	1.14	1.15	1.14	1.143	1.05	1.03	1.05	1.043
6	1.00	1.05	1.08	1.043	0.96	0.97	0.95	0.960
7	0.96	0.96	0.96	0.960	0.92	0.92	0.93	0.923
8	0.95	0.96	0.95	0.953	0.89	0.89	0.87	0.883
9	0.92	0.93	0.92	0.923	0.83	0.82	0.83	0.827
10	0.89	0.88	0.88	0.883	0.81	0.82	0.80	0.810
11	0.86	0.85	0.85	0.853	0.78	0.77	0.78	0.777
12	0.82	0.83	0.83	0.827	0.73	0.74	0.73	0.733
13	0.83	0.82	0.82	0.823	0.74	0.74	0.73	0.737
14	0.82	0.81	0.81	0.813	0.74	0.75	0.74	0.743
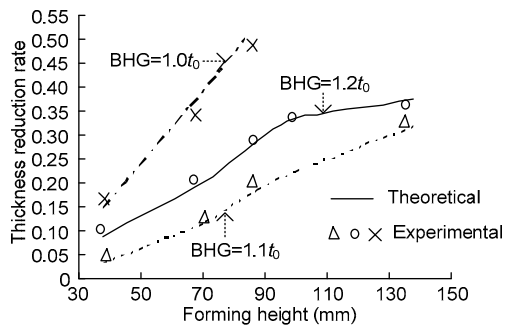
Fig. 18 Curves of reduction rate in the forming process
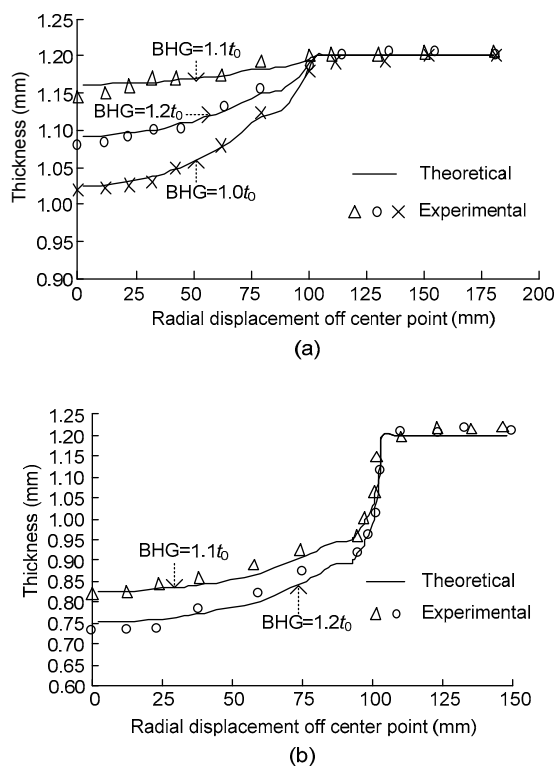

Fig. 19 Thickness distribution curves of workpieces
(a) *H*=38 mm; (b) *H*=138 mm

Comparing the results of Figs. 15 and 18, the maximum thickness reduction rate of the formed workpiece increases with the decrement of drawing weight. Combined with the experimental results in Tables 2 and 3, the thickness difference of the formed workpiece can be efficiently reduced and the forming height limit can also be improved in the deformation process of SGMF by setting reasonable blank holder and lubrication conditions, lowering the blank flow resistance and increasing the proportion of the drawing weight.

It can be seen from Fig. 19 that thickness is gradually reduced from the fillet of the female die to the central position of the workpiece. The difference between experimental measurement results and theoretical calculation is not obvious, and the maximum relative error is less than 10%.

With BHG=1.1t_0, the experimental workpieces at different forming stages are shown in Fig. 20. The profiles of workpieces in the female die region at different forming stages are shown in Fig. 21.
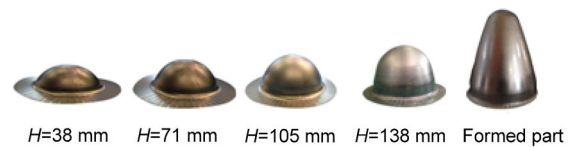

H=38 mm   *H*=71 mm   *H*=105 mm   *H*=138 mm   Formed part

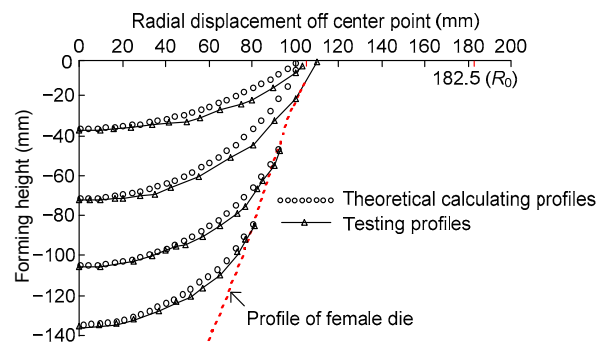**Fig. 20 Workpieces at different forming stages**

Fig. 21 Profiles of workpieces in the female die region at different forming stages

Comparing the calculated theoretical profiles and testing profiles in Fig. 21, we can see that there is little difference between two profile curves near the female die fillet when the forming height is small, while the two profile curves gradually coincide with the increase of the forming height. At an arbitrary forming stage, two profile curves coincide near the center point of the parts. With respect to Fig. 15, the bulging weight increases gradually and the bulging proportion increases in the whole deformation process with the increase of the forming height. Thus, the profile curve of the free deformation region is proximate to the spherical shell.

Under the same condition, the radial and tangential strain distributions of workpieces were obtained through theoretical calculation when the forming height is 38 mm or 138 mm (Fig. 22).
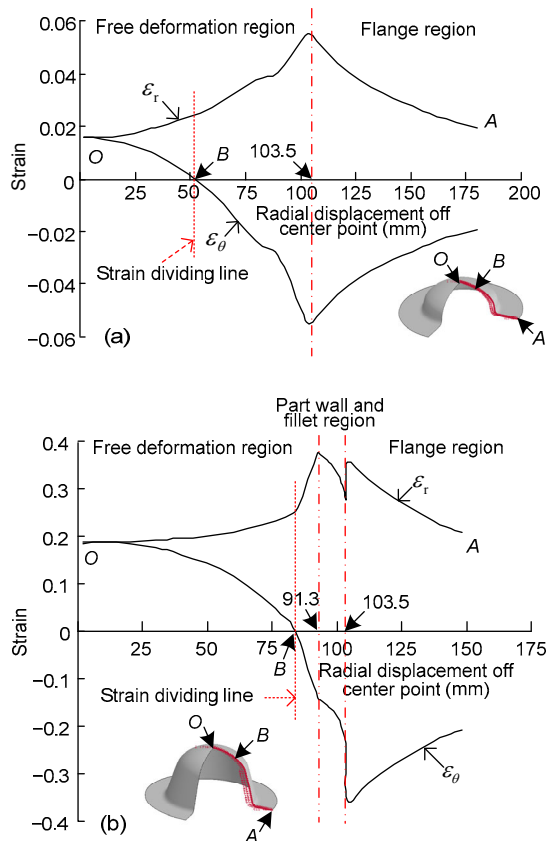
Fig. 22 Distributions of strain in the deformation process with forming height of 38 mm (a) or 138 mm (b)

It can be seen from Fig. 22 that the radial strain is the tensile strain and the tangential strain is the compressive strain in the flange region. From the outer edge of the flange to the female die fillet, the absolute value of the strain increases gradually. In the part wall and fillet region, the radial strain is the tensile strain and the tangential strain is the compressive strain. The absolute value of the tangential strain decreases gradually as the distance from the workpiece symmetry axis decreases. In the free deformation region, the radial strain decreases gradually and tangential strain transforms gradually from compressive strain to tensile strain. The radial strain equals the tangential strain near the symmetric axis of the workpiece.

Some conclusions can be drawn from the radial and tangential strain distribution curves. Before the part wall region is formed, as shown in Fig. 22a, the absolute values of the radial strain and tangential strain reach their maximum values simultaneously at the female die fillet. However, after the part wall region is formed, as shown in Fig. 22b, the absolute

value of the radial strain reaches its maximum value at the junction zone of the free deformation region and the part wall region, and the absolute value of the tangential strain reaches its maximum value at the female die fillet.

The strain dividing circle is defined as the set of points, on which the tangential strain is zero. As shown in Fig. 22a, the strain dividing circle locates in the free deformation region before the part wall region is formed. When the part wall region is formed, as shown in Fig. 22b, the female die deformation region is made up of the free deformation region and the part wall region. According to the geometrical conditions, the radius of the spherical cap of the free deformation region is 91.3 mm when the forming height is 138 mm. Thus, it can be seen from Fig. 22b that the strain dividing circle still locates in the free deformation region. Comparing Figs. 22a and 22b, the radius of the strain dividing circle increases gradually with the increase of the forming height; namely, the biaxial tensile strain region increases with the increase of the forming height.

From the analysis results of Fig. 15, the bulging weight increases gradually with the increase of forming height. Then the influence of bulging to the whole female die deformation increases, resulting in the enlargement of the biaxial tensile strain region. Therefore, the radius of the strain dividing circle gradually increases with the increase of the bulging weight, and the strain dividing circle moves toward to the lateral wall of the female die. In the forming process, an appropriate blank holder condition and a lubrication condition should be applied to increase the drawing weight and reduce the radius of the strain dividing circle, thus decreasing the biaxial tensile strain region at the bottom of the workpieces. Therefore, serious reduction of bottom blank thickness can be resisted and the limit forming height can be improved.

5 Conclusions

1. The deformation of sheet metal drawing in SGMF is a combination of drawing and bulging. The concepts of drawing weight and bulging weight are proposed as an original way of analyzing the forming process. The corresponding expressions are obtained.

The result shows that the larger the drawing weight is, the smaller the wall thickness difference of the formed workpiece becomes. This result is provided by the analysis of a parabolic part forming process. However, the effect of the bulging weight is opposite.

2. By analyzing the deformation of the flange region and the female die region of the parabolic part with drawing weight and bulging weight, the calculation formulas of strain in the deformation region for sheet metal drawing of SGMF are established. Also, the radius of the strain dividing circle can be calculated through the formulas. These concepts and formulas provide a new theory for analyzing sheet metal drawing of SGMF.

3. After the analysis of the parabolic part formed by drawing of SGMF, some design suggestions can be made. The forming height limit can be improved by setting reasonable forming conditions, increasing the drawing weight, and decreasing the radius of the strain dividing circle, which can also reduce the excessive thinning of the bottom.

References

Ahmetoglu, M., Jiang, H., Kulukuru, S., *et al.*, 2004. Hydro-forming of sheet metal using a viscous pressure medium. *Journal of Materials Processing Technology*, **146**(1): 97-107.
http://dx.doi.org/10.1016/S0924-0136(03)00849-5

Cao, M.Y., Zhao, C.C., Dong, G.J., 2012. Numerical simulation on granules medium drawing process parameters of magnesium alloy sheet. *Chinese Journal of Nonferrous Metals*, **22**(11):2992-2999 (in Chinese).

Dhaiban, A.A., Soliman, M.E.S., El-Sebaie, M.G., 2014. Finite element modeling and experimental results of brass elliptic cups using a new deep drawing process through conical dies. *Journal of Materials Processing Technology*, **214**(4):828-838.
http://dx.doi.org/10.1016/j.jmatprotec.2013.11.025

Dong, G.J., Zhao, C.C., Peng, Y.X., *et al.*, 2015. Hot granules medium pressure forming process of AA7075 conical parts. *Chinese Journal of Mechanical Engineering*, **28**(3): 580-591.
http://dx.doi.org/10.3901/CJME.2015.0217.019

Gavas, M., Izciler, M., 2006. Design and application of blank holder system with spiral spring in deep drawing of square cups. *Journal of Materials Processing Technology*, **171**(2):274-282.
http://dx.doi.org/10.1016/j.jmatprotec.2005.06.082

Grüner, M., Merklein, M., 2010. Numerical simulation of hydro forming at elevated temperatures with granular material used as medium compared to the real part geometry. *International Journal of Material Forming*, **3**(S1):279-282.
http://dx.doi.org/10.1007/s12289-010-0761-9

Gutscher, G., Wu, H.C., Ngaile, G., *et al.*, 2004. Determination of flow stress for sheet metal forming using the viscous pressure bulge (VPB) test. *Journal of Materials Processing Technology*, **146**(1):1-7.
http://dx.doi.org/10.1016/S0924-0136(03)00838-0

Halkaci, H.S., Turkoz, M., Dilmec, M., 2014. Enhancing formability in hydromechanical deep drawing process adding a shallow drawbead to the blank holder. *Journal of Materials Processing Technology*, **214**(8):1638-1646.
http://dx.doi.org/10.1016/j.jmatprotec.2014.03.008

Labergere, C., Gelin, J.C., 2012. Numerical simulation of sheet hydroforming taking into account analytical pressure and fluid flow. *Journal of Materials Processing Technology*, **212**(10):2020-2030.
http://dx.doi.org/10.1016/j.jmatprotec.2012.05.002

Li, Y.N., Luo, M., Gerlach, J., *et al.*, 2010. Prediction of shear-induced fracture in sheet metal forming. *Journal of Materials Processing Technology*, **210**(14):1858-1869.
http://dx.doi.org/10.1016/j.jmatprotec.2010.06.021

Liu, B.S., Lang, L.H., Zeng, Y.S., *et al.*, 2012. Forming characteristic of sheet hydroforming under the influence of through-thickness normal stress. *Journal of Materials Processing Technology*, **212**(9):1875-1884.
http://dx.doi.org/10.1016/j.jmatprotec.2012.03.021

Lücke, H.U., Hartl, C., Abbey, T., 2001. Hydroforming. *Journal of Materials Processing Technology*, **115**(1):87-91.
http://dx.doi.org/10.1016/S0924-0136(01)00774-9

Shulkin, L.B., Posteraro, R.A., Ahmetoglu, M.A., *et al.*, 2000. Blank holder force (BHF) control in viscous pressure forming (VPF) of sheet metal. *Journal of Materials Processing Technology*, **98**(1):7-16.
http://dx.doi.org/10.1016/S0924-0136(99)00300-3

Tari, D.G., Worswick, M.J., Winkler, S., 2013. Experimental studies of deep drawing of AZ31B magnesium alloy sheet under various thermal conditions. *Journal of Materials Processing Technology*, **213**(8):1337-1347.
http://dx.doi.org/10.1016/j.jmatprotec.2013.01.028

Thiruvarudchelvan, S., Tan, M.J., 2006. A note on fluid-pressure-assisted deep drawing processes. *Journal of Materials Processing Technology*, **172**(2):174-181.
http://dx.doi.org/10.1016/j.jmatprotec.2005.10.002

Wang, Z.J., Liu, J.G., Li, Y., 2010. Fracture prediction in non-isothermal viscous pressure bulging aluminum alloy sheet using ductile fracture criterion. *Journal of Central South University of Technology*, **17**(3):449-453.
http://dx.doi.org/10.1007/s11771-010-0505-5

Zhang, F.F., Li, X.F., Xu, Y.C., *et al.*, 2015. Simulating sheet metal double-sided hydroforming by using thick shell element. *Journal of Materials Processing Technology*, **221**:13-20.
http://dx.doi.org/10.1016/j.jmatprotec.2015.02.001

Zhao, C.C., 2005. Half-mould Forming Process for Metal Plate Material. China Patent 200510007167.1 (in Chinese).

Zhao, C.C., Wang, Y.S., Li, X.D., *et al.*, 2006. Experimental analysis of the pressure-carrying performance of solid granules medium. *Journal of Plasticity Engineering*, **13**(2):85-88 (in Chinese).

Zhao, C.C., Li, X.D., Dong, G.J., *et al.*, 2009. Solid granules medium forming technology and its numerical simulation. *Journal of Mechanical Engineering*, **45**(6):212-215 (in Chinese).

中文概要

题　目：抛物线型零件固体颗粒介质成形变形理论研究

目　的：板材固体颗粒介质成形工艺作为一种新型的软模成形技术，是采用固体颗粒代替刚性凸模或凹模(或弹性体、液体)对板料进行成形加工的工艺。固体颗粒介质板材拉深成形工艺为拉深和胀形两种变形模式的复合成形，其变形过程与传统拉深成形工艺有很大的区别。以抛物线型零件为研究对象，对其成形过程进行研究，建立固体颗粒介质板材软凸模拉深成形的几何条件和应变计算公式。

创新点：1. 首次提出了描述固体颗粒介质板材拉深成形变形机理的拉深权和胀形权的概念，并建立了相应的计算公式；2. 建立了固体颗粒介质抛物线型零件软凸模拉深成形的几何条件和应变计算公式。

方　法：1. 通过对抛物线型零件固体颗粒介质拉深成形的变形过程分析(图 1~3)，将变形过程和成形工件的变形区进行划分；2. 将数学中权函数的思想引入到对抛物线型零件固体颗粒介质拉深成形的分析中，提出拉深权和胀形权的定义及相应表达式(公式(1)和(2))；3. 通过理论推导，构建不同成形阶段抛物线型零件拉深成形过程中的应变计算式(公式(28)~(30)和公式(62a)~(62c))和壁厚计算公式(公式(31)和(63))；4. 利用 MATLAB 编制抛物线型零件拉深成形应变计算程序(图 14)；5. 以某航空零件为目标零件，通过试验试制不同成形条件下不同阶段的抛物线型工件(表 2 和 3)，将理论计算壁厚与实测厚度进行对比(图 19)，将试验轮廓与理论计算轮廓进行对比(图 21)，验证分析过程中所提假设及理论计算的可行性和正确性；将试验获得成形工件的几何尺寸(表 3)代入 MATLAB 计算程序中，对该航空零件的变形过程进行分析(图 15、18、19、21 和 22)。

结　论：1. 固体颗粒介质拉深成形过程是胀形和拉深的复合成形，通过对其变形过程分析，首次提出了拉深权和胀形权的概念，并且给出了其计算公式。成形过程中，拉深权越大，工件成形后的壁厚差越小；胀形权则正好相反。2. 利用拉深权和胀形权，建立了固体颗粒介质软凸模拉深成形变形区应变计算公式，且可以计算出应变分界圆位置半径，为分析固体颗粒介质软凸模拉深成形工艺变形过程提供了新的理论依据。3. 设置合理的成形条件、拉深权的提高和应变分界圆半径的缩小可以降低拉深成形过程中底部的过度减薄，进而提高极限成形高度。

关键词：固体颗粒介质；软模成形；拉深；拉深权；胀形权；应变